

1    **Nonlinear Electrophoresis of Microparticles in Shear Thinning Fluids**

2

3    Joseph Bentor, Chase Gabbard, Joshua B. Bostwick, and Xiangchun Xuan<sup>\*</sup>

4    Department of Mechanical Engineering, Clemson University, Clemson, SC 29634-0921, USA

5

---

<sup>\*</sup> Corresponding author. Email: [xcxuan@clemson.edu](mailto:xcxuan@clemson.edu) (Dr. Xuan).

1    **ABSTRACT**

2    The nonlinear electric field dependence of particle electrophoresis has been demonstrated to occur  
3    in Newtonian fluids for highly charged particles under large electric fields. It has also been  
4    predicted to arise from the rheological effects of non-Newtonian fluids even at small electric fields.  
5    We present in this work an experimental verification of nonlinear electrophoresis in shear thinning  
6    xanthan gum solutions through a straight rectangular microchannel. The addition of polymer into  
7    a Newtonian buffer solution is found to change the electric field dependence from linear to  
8    superlinear for electroosmotic, electrokinetic, and electrophoretic velocities. The nonlinear index  
9    of each of these electrokinetic phenomena increases with the increasing polymer or buffer  
10   concentration, among which electrophoresis exhibits the strongest nonlinearity. Both these  
11   observed trends are captured by a dimensionless electrokinetic shear thinning number that depends  
12   on the power-law index of fluid viscosity and the Debye length.

13

## 1 INTRODUCTION

2 Electrokinetic phenomena have been widely used to pump fluids and manipulate particles via  
3 electroosmosis and electrophoresis for microfluidic and nanofluidic applications.<sup>1-5</sup> The  
4 electrophoretic motion of a charged particle relative to a Newtonian electrolyte solution has a  
5 velocity proportional to the imposed electric field.<sup>6-8</sup> This regime of linear electrophoresis,  
6 however, breaks down for highly charged particles and/or large electric fields, where the non-  
7 uniformity of surface conduction in the Debye layer over the curved particle surface yields a  
8 superlinear electric field dependence of electrophoretic velocity.<sup>9-24</sup> Such a nonlinear  
9 electrophoretic behavior has also been predicted to occur in non-Newtonian fluids by several  
10 research groups.<sup>25</sup> Hsu and colleagues<sup>26-28</sup> reported that the numerically computed electrophoretic  
11 velocities of spherical and rod-shaped particles in shear thinning Carreau fluids are greater than in  
12 Newtonian fluids with the same zero-shear viscosities at the same electric fields. Moreover, the  
13 differences become more significant with the decreasing thickness of the Debye layer or  
14 equivalently the electric double layer (EDL). Khair *et al.*<sup>29</sup> presented a theoretical framework to  
15 calculate the electrophoretic velocity of a uniformly charged particle of any shape in both a power-  
16 law and a Carreau fluid. They demonstrated that the non-Newtonian contributions to  
17 electrophoretic motion from the Debye layer and bulk fluid, respectively, are each a nonlinear  
18 function of the electric field and particle zeta potential. The authors further pointed out that the  
19 Debye-layer contribution increases with the decreasing Debye length (because of, for example, the

1 increasing ionic concentration of the suspending fluid<sup>30,31</sup>) and the bulk-fluid contribution has an  
2 explicit dependence on particle size.

3 In another theoretical paper, Li and Koch<sup>32</sup> analyzed the electrophoretic motion of a weakly  
4 and uniformly charged particle in dilute viscoelastic polymer solutions under the thin EDL limit.  
5 They employed different constitutive equations to model the fluid elasticity with or without the  
6 shear thinning effects. Their Giesekus fluid (which is both viscoelastic and shear thinning<sup>33</sup>)-based  
7 model predicted that fluid elasticity decreases the electrophoretic velocity while shear thinning  
8 increases it, both of which show a second-order dependence on the applied electric field. Moreover,  
9 the authors noted that the elastic contribution to electrophoretic velocity has a quadratic  
10 dependence on the particle size, which has been experimentally verified by our group in a recent  
11 paper.<sup>34</sup> Among the three sizes of polystyrene microparticles under test, we observed that the larger  
12 particles move electrokinetically slower or alternatively electrophoretically faster than the smaller  
13 ones in viscoelastic polyethylene oxide (PEO) solutions though they have similar electrophoretic  
14 mobilities in the PEO-free Newtonian buffer solution. This particle size dependence increases with  
15 the increasing concentration and molecular weight of the PEO polymer because of the enhanced  
16 fluid elasticity as characterized by the increasing elasticity number. In addition, Ghosh and  
17 colleagues<sup>35,36</sup> analyzed the electrophoretic motion of a non-uniformed charge particle in an  
18 Oldroyd-B fluid (which is viscoelastic with a constant viscosity<sup>33</sup>) under the thin EDL limit. They  
19 revealed the particle size-dependence of both the electrophoretic velocity and trajectory.

1 In our recent experiment with viscoelastic PEO solutions,<sup>34</sup> we noticed an increasing deviation  
2 of electrophoretic particle motion from a linear trend of electric field with the increase of polymer  
3 concentration or molecular weight. These phenomena were speculated to result from the weak but  
4 increasing shear thinning effect of the PEO solutions. We present in this work the first  
5 experimental investigation of the sole effect of fluid shear thinning on electrophoretic as well as  
6 electroosmotic and electrokinetic velocities in xanthan gum (XG) solutions through a straight  
7 rectangular microchannel. We examine the impacts of both the polymer and buffer concentrations  
8 on the electric field dependence of each of these velocities. It is noted by the authors that the  
9 electroosmotic velocity of non-Newtonian fluids has been theoretically calculated using various  
10 constitutive equations,<sup>37-46</sup> among which the following formula characterizes the electroosmotic  
11 slip velocity,  $U_s$ , for power-law fluids in a slit microchannel under the Debye-Hückel  
12 approximation,<sup>47,48</sup>

$$13 \quad U_s = n\kappa^{\frac{1-n}{n}} \left( \frac{-\varepsilon\zeta E}{m} \right)^{\frac{1}{n}} \quad (1)$$

14 where  $n$  is the power-law index of fluid viscosity,  $\kappa$  is the inverse of Debye length,  $\varepsilon$  is the fluid  
15 permittivity,  $\zeta \leq \phi \cong 25$  mV is the wall zeta potential with  $\phi$  being the thermal voltage,  $E$  is the  
16 strength of the applied electric field, and  $m$  is the flow consistency index. The nonlinear  
17 dependence of  $U_s$  on both the applied electric field and wall zeta potential is qualitatively  
18 consistent with Khair *et al.*'s analysis of the electrophoretic velocity of particles in power-law  
19 fluids.<sup>29</sup> The prediction of eq 1 was, however, found to be significantly smaller than the

1 experimentally measured electroosmotic velocity of polymer solutions.<sup>48-50</sup> This discrepancy has  
2 been explained by the existence of a polymer depletion layer near the channel walls.<sup>48-52</sup>

3

4 **MATERIALS AND METHODS**

5 **Microchannel and Chemicals**

6 The experimental investigation was carried out utilizing a microfluidic device made from  
7 polydimethylsiloxane (PDMS) through the standard photo- and soft-lithography techniques as  
8 detailed in our prior work.<sup>53</sup> This device features a simple straight microchannel, which is 2 cm  
9 long with a rectangular cross section measuring 100  $\mu\text{m}$  in width and 50  $\mu\text{m}$  in depth. XG solutions  
10 were employed as the shear thinning fluid that has been reported to have a negligible elasticity  
11 effect.<sup>54,55</sup> They were prepared at three different concentrations, i.e., 1000 ppm, 2000 ppm and  
12 3000 ppm, by dissolving XG polymer (Tokyo Chemical Industry) into 0.1 mM phosphate buffer  
13 (specifically, 0.0754 mM disodium phosphate and 0.0246 mM monosodium phosphate, which  
14 may be viewed as a primarily uni-bivalent solution). The polymer-free (i.e., 0 ppm XG) pure buffer  
15 was also tested as a control experiment. The influence of ionic concentration on electrokinetic  
16 phenomena was explored in three types of 2000 ppm XG solutions, which were prepared in 0.01  
17 mM, 0.1 mM, and 1 mM phosphate buffers, respectively. For the electrophoresis experiment,  
18  $\mu\text{m}$ -diameter spherical polystyrene particles (Sigma-Aldrich) were re-suspended in each of the  
19 prepared XG solutions at a low volume fraction (< 0.1%) to minimize the particle-particle  
20 interaction.

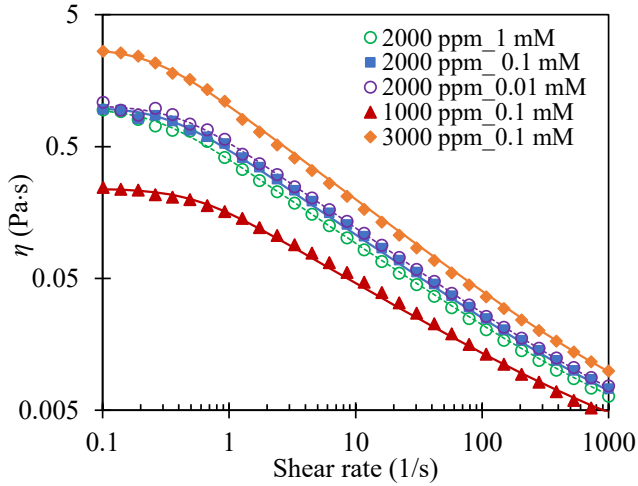


**Figure 1.** Experimentally measured (symbols) and Carreau-fluid model fitted (lines) viscosity data for XG solutions with varying polymer concentrations (i.e., 1000, 2000 and 3000 ppm) and prepared in phosphate buffers with varying ionic concentrations (i.e., 0.01, 0.1 and 1 mM).

The viscosity,  $\eta$ , of every prepared XG solution was measured using a cone-plate rheometer

(Anton Paar, MCR 302) at room temperature. The obtained data were fitted to the Carreau-fluid

model using the least-squares method as depicted in Figure 1,

$$\frac{\eta - \eta_\infty}{\eta_0 - \eta_\infty} = [1 + (\lambda_C \dot{\gamma})^2]^{(n-1)/2} \quad (2)$$

where  $\eta_\infty$  is the infinite-shear-rate viscosity,  $\eta_0$  is the zero-shear-rate viscosity,  $\lambda_C$  is a time constant,  $\dot{\gamma}$  is the fluid shear rate, and  $n$  is the power-law index identical to that defined in eq 1.

Table 1 summarizes the obtained fitting parameters for the Carreau-fluid model, each of which has

an uncertainty of no more than 5%. We see that increasing the XG concentration significantly

increases the dynamic viscosity and enhances the fluid shear thinning effect because of the lowered

value of  $n$ . In contrast, increasing the buffer concentration causes a slight decrease in both the

dynamic viscosity and shear thinning effect. It also reduces the Debye length,  $1/\kappa$ , and in turn the

dimensionless EDL thickness,  $1/\kappa a$ , with respect to the particle radius  $a$ , which will be used later

1 in the discussion of the experimental results. Referring to the seminal paper from Henry (see Table  
2 1 therein),<sup>56</sup> we set  $1/\kappa \approx 56$  nm for 0.01 mM phosphate buffer that is viewed as a uni-bivalent  
3 solution as noted above. The values of the Debye length in 0.1 mM and 1 mM buffers were then  
4 calculated using its inverse scaling with the square root of the buffer concentration.<sup>30,31</sup>

5  
6 **Table 1.** Rheological properties of the prepared XG solutions obtained from the fitting of the  
7 experimentally measured viscosity data in Figure 1 with the Carreau-fluid model in eq 2.

8

XG conc.	2000 ppm		1000 ppm		3000 ppm
Buffer conc.	1 mM	0.1 mM	0.01 mM	0.1 mM	0.1 mM
$\eta_0$ (Pa·s)	0.98	1.0	1.03	0.24	2.8
$\eta_\infty$ (Pa·s)	$2.0 \times 10^{-3}$	$2.0 \times 10^{-3}$	$2.0 \times 10^{-3}$	$1.6 \times 10^{-3}$	$2.7 \times 10^{-3}$
$\lambda_C$ (s)	3.9	3.0	2.5	1.9	4.0
$n$	0.35	0.34	0.33	0.43	0.28
$1/\kappa$ (nm)	5.6	18	56	18	18
$n(\kappa a)^{(1-n)/n}$	29000	5100	740	300	94400

9  
10 **Experimental Techniques**  
11 DC electric fields were used to drive the prepared XG and buffer solutions through the  
12 microchannel for the electroosmotic fluid velocity measurement. They were also used to drive the  
13 particle suspension in each of the prepared solutions for the electrokinetic particle velocity  
14 measurement. The liquid heights in the two end-channel reservoirs were carefully balanced prior  
15 to each test to minimize the influence of hydrostatic pressure-induced fluid flow. Electric voltages  
16 ranging from 200 to 800 V were applied using a DC power source (Glassman High Voltage, Inc.),

1 yielding average electric field from 100 to 400 V/cm across the 2 cm long microchannel. The effect  
2 of Joule heating was estimated insignificant over this range of electric fields as the electric current  
3 was observed to remain nearly constant during each test.<sup>57</sup> Note this estimation is only valid for  
4 buffer solutions that have a temperature dependent electric conductivity.<sup>58</sup> The dimensionless  
5 electric field,  $Ea/\phi$  with  $\phi$  being the thermal voltage as noted earlier, was calculated to be no  
6 more than 4 for 5  $\mu\text{m}$  particles at the highest electric field of 400 V/cm, which, as demonstrated in  
7 our recent papers,<sup>59,60</sup> is not large enough to induce nonlinear electrophoresis.

8 The electroosmotic velocity of each prepared solution,  $V_{eo}$ , was measured using the electric  
9 current monitoring technique,<sup>61</sup> which was performed by connecting a digital multimeter (Siglent  
10 SDM3045X) in series with the microchannel. Briefly, the time response of the current variation  
11 was recorded when a test solution was electroosmotically displaced by an auxiliary solution with  
12 90% ionic concentration of the former. The slope of this time development for electric current was  
13 then input into a theoretical formula to compute the electroosmotic velocity. This measurement  
14 was repeated at least twice for each solution at each electric field ranging from 100 to 400 V/cm  
15 with the goal to achieve a statistical verification of the observed linear or nonlinear phenomena.  
16 The electrokinetic motion of particles,  $V_{ek}$ , was recorded in the middle of the microchannel using  
17 a microscope (Nikon Eclipse TE2000U, Nikon Instruments) equipped with a CCD camera (Nikon  
18 DS-Qi1Mc). It was observed in our experiment to align with the direction of the applied DC  
19 electric field and hence that of  $V_{eo}$  in all the prepared particle suspensions. This phenomenon

1 indicates that  $V_{eo}$  is greater than the opposing electrophoretic motion of particles,  $V_{ep}$ , in our  
2 experiment, leading to,

3 
$$V_{ep} = V_{eo} - V_{ek} \quad (3)$$

4 The pressure-driven return flow induced by the electroosmotic fluid depletion/buildup in the  
5 reservoirs is not considered in eq 3, which has been proved reasonable in our recent  
6 experiments<sup>59,60</sup> as long as the duration of each test was kept short (no more than 30 s in this study).

7 The captured particle images were processed using the Nikon imaging software (NIS-Elements  
8 AR 2.30). The value of  $V_{ek}$  was determined using the ImageJ software (National Institutes of  
9 Health), where around twenty particles were tracked in each case to obtain the average velocity.  
10 The largest positive and negative deviations of all the measured particle velocities from the average  
11 were then used to determine the experimental error bar. This process was also repeated at least  
12 twice to achieve a statistical verification of the observed linear or nonlinear particle velocity. As  
13 an inclined migration of particles towards the channel walls was noticed in XG solutions like what  
14 we reported in an earlier paper,<sup>62</sup> we considered only those particles traveling near the channel  
15 centerline to minimize the potential influence of particle position on the velocity measurement.

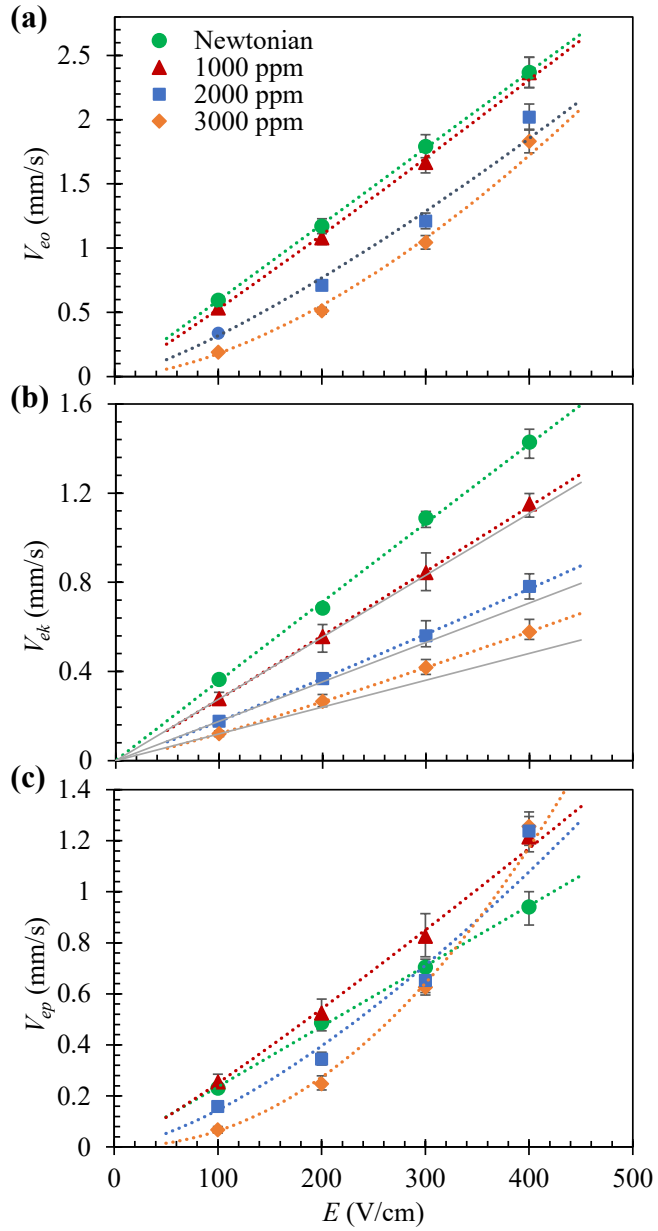
16

17 **RESULTS AND DISCUSSION**

18 **Effect of Polymer Concentration**

19 Figure 2a shows the experimentally measured electroosmotic velocities,  $V_{eo}$ , in 0.1 mM phosphate  
20 buffer-based 1000/2000/3000 ppm XG solutions and the pure buffer solution. The addition of XG

1 polymer into the buffer solution reduces the value of  $V_{eo}$ , which gets more significant with the  
2 increase of XG concentration. This observation is attributed to the increasingly larger contribution  
3 of polymer viscosity to the total fluid viscosity (see Figure 1). However, in line with previous  
4 studies,<sup>48-52</sup> we find that the discrepancy of  $V_{eo}$  in between XG (e.g., 1000 ppm) and Newtonian  
5 buffer solutions in our experiment is also much smaller than that of their viscosities. Specifically,  
6 the viscosity of the Newtonian buffer is assumed equal to that of water at  $1.0 \times 10^{-3}$  Pa·s while that  
7 of 1000 ppm XG is about 20 times larger. The latter value was estimated from the viscosity plot  
8 in Fig. 1 using the calculated shear rate,  $\dot{\gamma} = 2V_{eo}/d$  with  $d = 50$   $\mu\text{m}$  being the channel depth, for  
9 the experimentally measured  $V_{eo} \approx 1$  mm/s at 200 V/cm in Fig. 2. Such a phenomenon has been  
10 explained in previous studies using an assumed polymer depletion layer on the channel walls,<sup>48-52</sup>  
11 wherein the solution behaves like a polymer-free Newtonian fluid leading to a locally reduced  
12 drag. The formation of such a layer may be attributed to the negative surface charge of both the  
13 channel walls and the carboxyl groups of XG polymer molecules. Another trend we view from  
14 Figure 2a is that adding XG polymer into the buffer solution changes the dependence of  $V_{eo}$  on the  
15 applied electric field from linear to superlinear. Moreover, the nonlinearity gets stronger in higher-  
16 concentration XG solutions, which should result from the enhanced shear thinning effect therein  
17 (see the value of power-law index,  $n$ , in Table 1). A quantitative analysis of the nonlinearity in  
18 electroosmotic fluid flow will be presented later along with that in electrokinetic/electrophoretic  
19 particle motion.



1  
2 **Figure 2.** Polymer concentration effects on the experimentally measured (symbols with error bars)  
3 electroosmotic fluid velocity (a),  $V_{eo}$ , electrokinetic particle velocity (b),  $V_{ek}$ , and electrophoretic  
4 particle velocity (c),  $V_{ep}$ , in shear thinning XG and Newtonian buffer (i.e., 0 ppm XG) solutions.  
5 The ionic concentration is fixed at 0.1 mM in all solutions. The dashed lines are each either a  
6 power (for XG solutions) or a linear (for Newtonian buffer solution) fit to the experimental data.  
7 The solid gray lines in (b) are each a linear trendline passing through the data point at 100 V/cm  
8 for every XG solution and the origin.

9

1      Figure 2b compares the experimentally measured electrokinetic velocities,  $V_{ek}$ , of 5  $\mu\text{m}$ -  
2      diameter particles in 1000/2000/3000 ppm XG solutions and pure buffer solution. Similar to the  
3      observation of  $V_{eo}$  in Figure 2a,  $V_{ek}$  also decreases with the increasing XG concentration whose  
4      extent, however, still turns out much weaker than the corresponding increase of fluid viscosity  
5      because of perhaps the formation of a polymer depletion layer near the particle surface. Moreover,  
6      like  $V_{eo}$ , adding XG polymer into the buffer solution causes a superlinear electric field-dependence  
7      of  $V_{ep}$  that increases in higher-concentration XG solutions. Figure 2c shows the electrophoretic  
8      particle velocity,  $V_{ep}$ , obtained from the experimental data in Figures 2a and 2b via eq 3. Consistent  
9      with the classical electrokinetic theory,<sup>6-8</sup> the data for  $V_{ep}$  in the Newtonian buffer solution follow  
10     a linear relationship with respect to the applied electric field. In contrast, those for  $V_{ep}$  in XG  
11     solutions exhibit an increasingly nonlinear upward trend. Consequently,  $V_{ep}$  in 3000 ppm XG  
12     solution can surpass that in 1000 ppm solution at 400 V/cm though it is much less than the latter  
13     at 100 V/cm. This phenomenon may be associated with the nonlinear dependence of  $V_{ep}$  on the  
14     electric field and particle zeta potential (like  $V_{eo}$  in eq 1), both of which increase with the stronger  
15     fluid shear thinning effect in the higher-concentration XG solution.

16

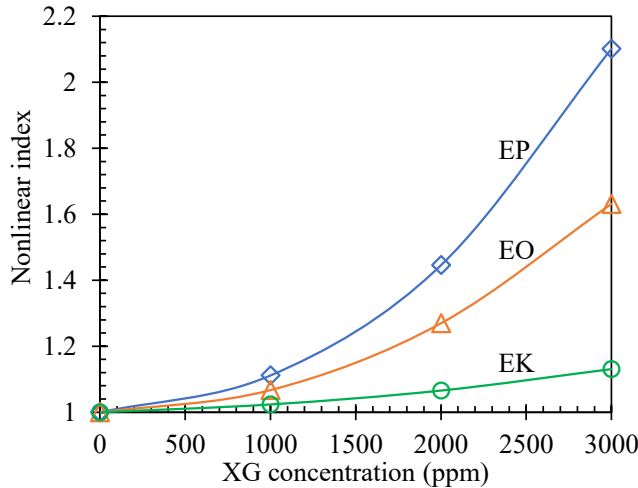


**Figure 3.** Polymer concentration effects on the nonlinear index (obtained from the power trendlines fitted to the data points in Figure 2) for the electric field dependence of electrophoretic (EP), electroosmotic (EO), and electrokinetic (EK) velocities in 0.1 mM buffer based XG solutions. Note that 0 ppm XG indicates the pure buffer solution, and the lines are used to guide the eyes only.

To quantify the influence of XG concentration on the electric field-dependences of  $V_{eo}$ ,  $V_{ek}$  and  $V_{ep}$ , we fit the data points for each XG solution in Figures 2a, 2b and 2c, respectively, to a power trendline. A comparison of the indices of these trendlines, named as nonlinear index following our previous studies,<sup>58,59</sup> is presented in Figure 3. We see that increasing the polymer concentration strengthens the nonlinearity in each electrokinetic phenomenon because of the enhanced fluid shear thinning effect. Moreover,  $V_{ep}$  has the largest nonlinear index among the three velocities in each XG solution, which is followed by  $V_{eo}$  and  $V_{ek}$  in order. Specifically, the nonlinear index for  $V_{eo}$  increases from 1 (i.e., linear) in the Newtonian buffer solution to 1.02, 1.27 and 1.63 in 1000, 2000 to 3000 ppm XG solutions, respectively. The three nonlinear indices are each much smaller than the theoretically predicted values of 2.33, 2.94 and 3.57 based on  $1/n$  in

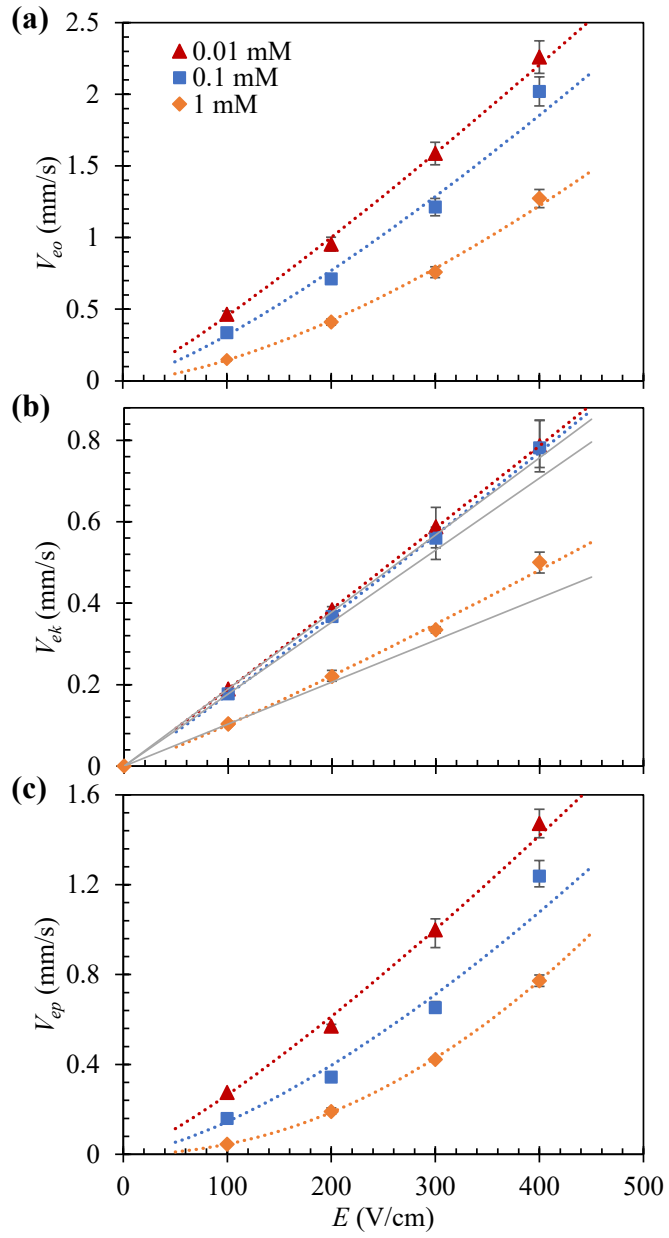
1 eq 1. This discrepancy may arise from three factors: (1) the theory considers a slit microchannel  
2 and hence underestimates the wall effects on the electroosmotic flow in a rectangular  
3 microchannel; (2) the theory employs a power-law fluid model, which may overestimate the shear  
4 thinning effect of a Carreau-like fluid in our experiment; (3) the theory ignores the polymer  
5 depletion layer, which may again overestimate the shear thinning effect because of the  
6 overestimated fluid drag from the channel walls. We attribute the greater nonlinear index for  $V_{ep}$   
7 than that for  $V_{eo}$  to the curvature of particle surface such that the fluid shear rate variation gets  
8 enhanced around a particle. The weakest nonlinearity for  $V_{ek}$  results from the opposing directions  
9 of  $V_{eo}$  and  $V_{ep}$ , between which the former has a greater magnitude in all tested XG solutions.

10

## 11 **Effect of Buffer Concentration**

12 Figure 4a shows the experimentally measured values for  $V_{eo}$  in 0.01, 0.1 and 1 mM phosphate  
13 buffer-based 2000 ppm XG solutions. Decreasing the buffer concentration significantly increases  
14  $V_{eo}$  at each applied electric field because the negative surface charge on the PDMS and glass walls  
15 increases as a result of the reduced counterion adsorption to the substrate surface.<sup>63</sup> This trend is  
16 not significantly affected by the slightly increased XG solution viscosity in a lower-concentration  
17 buffer solution (see Figure 1), which should in theory reduce the magnitude of  $V_{eo}$ . Decreasing the  
18 buffer concentration also weakens the superlinear dependence of  $V_{eo}$  on the applied electric field.  
19 This trend goes against the slightly enhanced fluid shear thinning effect (in terms of a smaller  
20 power-index,  $n$ , in Table 1) in XG solutions prepared in lower-concentration buffers. It should be

1 attributed to the increasing EDL thickness in terms of the Debye length,  $1/\kappa$  (see the values in  
2 Table 1), which is speculated to expand the polymer depletion layer near the channel walls because  
3 of the action of the intrinsic electric field within the EDL<sup>6-8</sup> upon the negatively charged XG  
4 polymer molecules. The enhanced cross-stream migration of polymers towards the bulk because  
5 of the stronger electroosmotic shear flow near the walls<sup>64</sup> in a lower-concentration buffer may also  
6 play a role here. Consequently, the working range of fluid shear thinning in XG solutions is  
7 suppressed with the decrease of buffer concentration.



1  
2 **Figure 4.** Buffer concentration effects on the experimentally measured (symbols with error bars)  
3 electroosmotic fluid velocity (a),  $V_{eo}$ , electrokinetic particle velocity (b),  $V_{ek}$ , and electrophoretic  
4 particle velocity (c),  $V_{ep}$ , in 2000 ppm XG solutions. The dashed lines are each a power fit to the  
5 experimental data. The solid gray lines in (b) are each a linear trendline passing through the data  
6 point at 100 V/cm for every XG solution and the origin.

1      Figure 4b shows the experimentally measured  $V_{ek}$  of 5  $\mu\text{m}$ -diameter particles in 0.01, 0.1 and  
2      1 mM phosphate buffer-based 2000 ppm XG solutions. A similar trend to  $V_{eo}$  in Figure 4a is  
3      observed for  $V_{ek}$  that increases as the buffer concentration decreases. Meanwhile,  $V_{ek}$  also exhibits  
4      a weakened superlinear dependence on the applied electric field. Figure 4c shows the calculated  
5       $V_{ep}$  of 5  $\mu\text{m}$ -diameter particles from eq 3 using the experimental data in Figures 4a and 4b. Similar  
6      trends to  $V_{eo}$  and  $V_{ek}$  are noted for  $V_{ep}$  because of the same reasons for  $V_{eo}$  as noted above. Figure  
7      5 compares the extracted values of nonlinear index for the electric field dependence of these three  
8      velocities, among which  $V_{ep}$  still has the largest value like Figure 3. The nonlinear index increases  
9      with the increasing buffer concentration for each velocity. This phenomenon is qualitatively  
10     consistent with the Carreau fluid-based theoretical analysis in the literature.<sup>26-29</sup> It also seems to  
11     correlate well with the experiment from Chang and Tsao,<sup>50</sup> who reported that the addition of salt  
12     can enhance the drag reduction in the electroosmotic flow of polymer solutions because of the  
13     reduced EDL thickness.

14

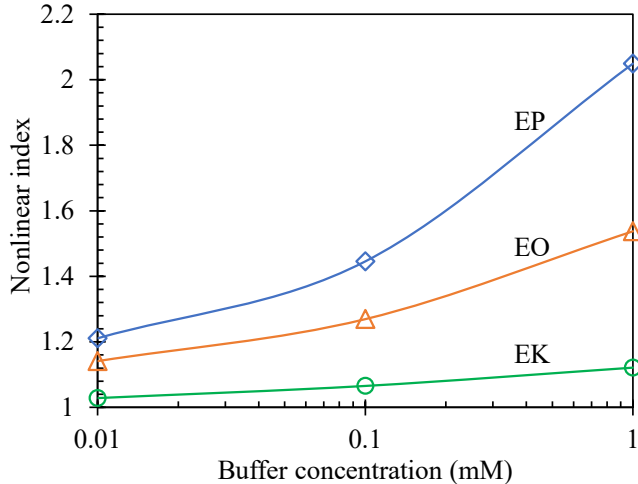


**Figure 5.** Buffer concentration effects on the nonlinear index (obtained from the power trendlines fitted to the data points in Figure 4) for the electric field dependence of electrophoretic (EP), electroosmotic (EO), and electrokinetic (EK) velocities, respectively, in 2000 ppm XG solutions. Note that the lines are used to guide the eyes only.

## Summary of the Nonlinear Index

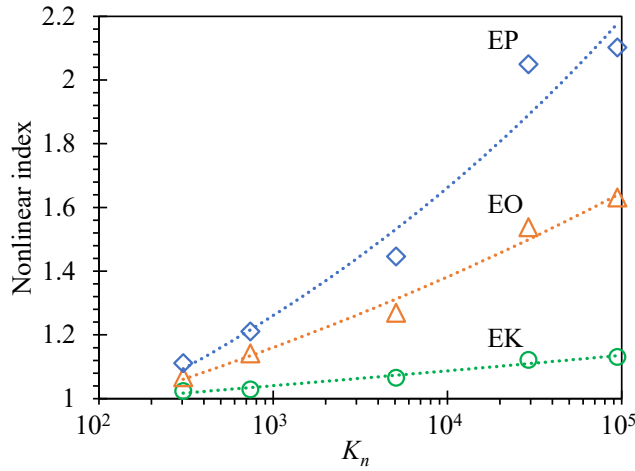
To put together the above presented results for the effects of polymer concentration (Figure 3) and buffer concentration (Figure 5) into one plot for a unified understanding, we rewrite the electroosmotic slip velocity of power-law fluids in eq 1 as,

$$U_s = n(\kappa a)^{\frac{1-n}{n}} \left[ a \left( \frac{-\varepsilon \zeta E}{ma} \right)^{\frac{1}{n}} \right] = K_n \left[ a \left( \frac{-\varepsilon \zeta E}{ma} \right)^{\frac{1}{n}} \right] \quad (4)$$

where the pre-factor  $K_n = n(\kappa a)^{(1-n)/n}$  is dimensionless and can be used to characterize the fluid shear thinning effects on electrokinetic phenomena. Hence, we term  $K_n$  the electrokinetic shear thinning number, which is a strong function of both the power-law index,  $n$ , and the Debye length,  $1/\kappa$ . Figure 6 demonstrates that with the increase of  $K_n$  (see its values in the last row of Table 1), the nonlinear index exhibits an increasing trend for  $V_{ep}$ ,  $V_{eo}$  and  $V_{ek}$  in our tested XG solutions.

1 Moreover, each of these trends can be best fitted to a power trendline with a better than 95% R-  
 2 Squared value. It is important to note that the length scale introduced in  $K_n$ , i.e., the particle radius,  
 3  $a$ , in eq 4, needs to satisfy the condition,  $\kappa a \gg 1$ , because otherwise the impact of buffer  
 4 concentration in terms of  $\kappa \sim O(10^8) \text{ m}^{-1}$  in the original pre-factor of  $U_s$  in eq 1 will be  
 5 significantly underestimated. For example, it is natural to use the radius of gyration of the XG  
 6 polymer,  $R_g$  (reported to be on the order of 100 nm<sup>65,66</sup>), to replace the particle radius,  $a$ , in eq 4  
 7 as the former length scale has been reported to correlate with the polymer depletion layer.<sup>48-52</sup>  
 8 However,  $\kappa R_g \gg 1$  may become invalid and hence not be used to define the electrokinetic shear  
 9 thinning number.

10



11  
 12 **Figure 6.** The experimentally determined nonlinear index (symbols) for the electric field  
 13 dependence of electrophoretic (EP), electroosmotic (EO), and electrokinetic (EK) velocities,  
 14 respectively, as a function of the electrokinetic shear thinning number,  $K_n = n(\kappa a)^{(1-n)/n}$   
 15 (reduced to 1 for the Newtonian buffer, see Table 1 for the values in our prepared XG solutions).  
 16 The dashed lines are each a power fit to the data points.

17

## 1 CONCLUSIONS

2 We have conducted an experimental study of the electrokinetic phenomena in shear thinning XG  
3 solutions through a rectangular microchannel. Adding polymer into the Newtonian buffer is found  
4 to reduce  $V_{eo}$  and  $V_{ek}$  because of the additional contribution of polymer viscosity to the total fluid  
5 viscosity. It also changes the electric field dependence of both velocities from linear to superlinear,  
6 leading to nonlinear  $V_{ep}$  even at small electric fields because of the induced fluid shear thinning  
7 effect. Our analysis reveals that  $V_{ep}$  has the largest nonlinear index followed by  $V_{eo}$  and  $V_{ek}$  in  
8 order because the fluid shear rate variation and hence the shear thinning effect gets locally  
9 enhanced around the curved particle surface. Moreover, the nonlinear index of each of these  
10 electrokinetic phenomena increases with the increasing polymer or buffer concentration. The  
11 former trend can be attributed to the strengthened fluid shear thinning effect while the latter is  
12 associated with the reduced EDL thickness and qualitatively consistent with earlier studies.<sup>26-29,50</sup>  
13 We have also introduced a dimensionless electrokinetic shear thinning number to characterize the  
14 combined effects of polymer and buffer concentrations on the nonlinear index. For future work we  
15 will investigate if the nonlinear index of  $V_{ep}$  depends on particle size in XG solutions, or in other  
16 words if fluid shear thinning causes the particle size dependence of  $V_{ep}$  like fluid elasticity in our  
17 recent work,<sup>34</sup> enabling an electrophoretic separation of particles by size. It is envisioned that the  
18 combination of fluid rheology with nonlinear electrophoresis<sup>21</sup> and dielectrophoresis<sup>67,68</sup> will  
19 further broaden the application of nonlinear electrokinetic methods<sup>69</sup> in micro/nanofluidic particle  
20 manipulations.

1

2 **ACKNOWLEDGEMENTS**

3 This work was supported in part by NSF under grant numbers CBET-2100772 and CBET-  
4 2127825.

5

6 **REFERENCES**

7 [1] Xuan, X. Recent advances in direct current electrokinetic manipulation of particles for  
8 microfluidic applications. *Electrophoresis* **2019**, *40*, 2484–2513.

9 [2] Uematsu, Y.; Ohshima, H. Electrophoretic mobility of a water-in-oil droplet separately  
10 affected by the net charge and surface charge density. *Langmuir* **2022**, *38*, 4213–4221.

11 [3] Ahmadi, E.; Sadeghi, A.; Chakraborty, S. Slip-coupled electroosmosis and electrophoresis  
12 dictate DNA translocation speed in solid-state nanopores. *Langmuir* **2023**, *39*, 12292–  
13 12301.

14 [4] Song, Y.; Li, D.; Xuan, X. Recent advances in multi-mode microfluidic separation of  
15 particles and cells. *Electrophoresis* **2023**, *44*, 910–937.

16 [5] Dang, V.-T.; Pham, V.-S. Determination of critical dimensions of microchannels to ensure  
17 the electrokinetic biomolecule preconcentration: Analytical and numerical studies.  
18 *Langmuir* **2024**, *40*, 6051–6064.

19 [6] Hunter, R. J. *Zeta Potential in Colloid Science*. New York, Academic Press, 1981.

1 [7] Lyklema, J. *Fundamentals of Interface and Colloid Science*. Cambridge, MA, Academic  
2 Press, 1991.

3 [8] Masliyah, J. H.; Bhattacharjee, S. *Electrokinetic and Colloid Transport Phenomena*.  
4 Hoboken, New Jersey, Wiley-Interscience, 2006.

5 [9] O'Brien, R. W.; White, L. R. Electrophoretic mobility of a spherical colloidal particle. *J.  
6 Chem. Soc. Faraday Trans.* **1978**, *74*, 1607-1626.

7 [10] Dukhin, S. S. Electrophoresis at large peclet numbers. *Adv. Colloid Interface Sci.* **1991**, *6*,  
8 219-248.

9 [11] Mishchuk, N. A.; Dukhin, S. S. Electrophoresis of solid particles at large Peclet  
10 numbers. *Electrophoresis* **2002**, *23*, 2012–2022.

11 [12] Shilov, V.; Barany, S.; Grosse, C.; Shramko, O. Field-induced disturbance of the double  
12 layer electro-neutrality and non-linear electrophoresis. *Adv. Colloid Interface Sci.* **2003**,  
13 *104*, 159–173.

14 [13] Barany, S. Electrophoresis in strong electric fields. *Adv. Colloid Interface Sci.* **2009**, *147–  
15 148*, 36–43.

16 [14] Mishchuk, N. A. Concentration polarization of interface and non-linear electrokinetic  
17 phenomena. *Adv. Colloid Interface Sci.* **2010**, *160*, 16-39.

18 [15] Schnitzer, O.; Zeyde, R.; Yavneh, I.; Yariv, E. Weakly nonlinear electrophoresis of a highly  
19 charged colloidal particle. *Phys. Fluids* **2013**, *25*, 052004.

1 [16] Schnitzer, O.; Yariv, E. Nonlinear electrophoresis at arbitrary field strengths: small-  
2 Dukhin-number analysis. *Phys. Fluids* **2014**, *26*, 122002.

3 [17] Youssefi, M. R.; Diez, F. J. Ultrafast electrokinetics. *Electrophoresis* **2016**, *37*, 692-698.

4 [18] Tottori, S.; Misiunas, K.; Keyser, U. F. Nonlinear electrophoresis of highly charged  
5 nonpolarizable particles. *Phys. Rev. Lett.* **2019**, *123*, 014502.

6 [19] Antunez-Vela, S.; Perez-Gonzalez, V. H.; De Peña, A. C.; Lentz, C. J.; Lapizco-Encinas, B.  
7 H. Simultaneous determination of linear and nonlinear electrophoretic mobilities of cells  
8 and microparticles. *Anal. Chem.* **2020**, *92*, 14885–14891.

9 [20] Vaghef-Koodehi, A.; Dillis, C.; Lapizco-Encinas, B. H. High-resolution charge-based  
10 electrokinetic separation of almost identical microparticles. *Anal. Chem.* **2022**, *94*, 6451-  
11 6456.

12 [21] Khair, A. S. Nonlinear electrophoresis of colloidal particles. *Current Opinion Colloid  
13 Interface Sci.* **2022**, *59*, 101587.

14 [22] Cobos, R.; Khair, A. S. Nonlinear electrophoretic velocity of a spherical colloidal particle.  
15 *J. Fluid Mech.* **2023**, *968*, A14.

16 [23] Ernst, O. D.; Vaghef-Koodehi, A.; Dillis, C.; Lomeli-Martin, A.; Lapizco-Encinas, B. H.  
17 Dependence of nonlinear electrophoresis on particle size and charge. *Anal. Chem.* **2023**,  
18 *95*, 6595–6602.

1 [24] Lomeli-Martin, A.; Ernst, O. D.; Cardenas-Benitez, B.; Cobos, R.; Khair, A. S.; Lapizco-  
2 Encinas, B. H. Characterization of the nonlinear electrophoretic behavior of colloidal  
3 particles in a microfluidic channel. *Anal. Chem.* **2023**, *95*, 6740–6747.

4 [25] Zhao, C.; Yang, C. Advances in electrokinetics and their applications in micro/nano fluidics.  
5 *Microfluid Nanofluid.* **2012**, *13*, 179-203.

6 [26] Lee, E.; Tsai, C. S.; Hsu, J.; Chen, C. J. Electrophoresis in a Carreau fluid at arbitrary zeta  
7 potentials. *Langmuir* **2004**, *20*, 7952–7959.

8 [27] Hsu, J. P.; Yeh, L. H.; Ku, M. H. Electrophoresis of a spherical particle along the axis of a  
9 cylindrical pore filled with a Carreau fluid. *Colloid Polym. Sci.* **2006**, *284*, 886–892.

10 [28] Yeh, L. H.; Hsu, J. P. Electrophoresis of a finite rod along the axis of a long cylindrical  
11 microchannel filled with Carreau fluids. *Microfluid. Nanofluid.* **2009**, *7*, 383–392.

12 [29] Khair, A. S.; Posluszny, D. E.; Walker, L. M. Coupling electrokinetics and rheology:  
13 Electrophoresis in non-Newtonian fluids. *Phys. Rev. E* **2012**, *85*, 016320.

14 [30] Li, D. *Electrokinetics in Microfluidics*. Burlington, MA, Elsevier Academic Press, 2004.

15 [31] Chang, H. C.; Yeo, L. Y. *Electrokinetically Driven Microfluidics and Nanofluidics*. New  
16 York, Cambridge University Press, 2010.

17 [32] Li, G.; Koch, D. L. Electrophoresis in dilute polymer solutions. *J. Fluid Mech.* **2020**, *884*,  
18 A9.

19 [33] Bird, R. B.; Wiest, J. M. Constitutive equations for polymeric liquids. *Annu. Rev. Fluid  
20 Mech.* **1995**, *27*, 169-193.

1 [34] Bentor, J.; Xuan, X. Particle size-dependent electrophoresis in polymer solutions. *Anal.*  
2 *Chem.* **2024**, *96*, 3186-3191.

3 [35] Ghosh, U.; Mukherjee, S.; Chakraborty, S. Electrophoretic motion of a non-uniformly  
4 charged particle in a viscoelastic medium in thin electrical double layer. *J. Fluid Mech.*  
5 **2021**, *924*, A41.

6 [36] Borthakur, R.; Ghosh, U. Electrophoretic trajectories of non-uniformly charged particles  
7 in viscoelastic fluids: the weak surface charge limit. *J. Fluid Mech.* **2023**, *954*, A48.

8 [37] Das, S.; Chakraborty, S. Analytical solutions for velocity, temperature and concentration  
9 distribution in electroosmotic microchannel flows of a non-Newtonian bio-fluid. *Anal.*  
10 *Chim. Acta* **2006**, *559*, 15–24.

11 [38] Berli, C. L. A.; Olivares, M. L. Electrokinetic flow of non-Newtonian fluids in  
12 microchannels. *J. Colloid Interface Sci.* **2008**, *320*, 582–589.

13 [39] Zhao, C.; Yang, C. An exact solution for electroosmosis of non-Newtonian fluids in  
14 microchannels. *J. Non-Newton. Fluid Mech.* **2011**, *166*, 1076–1079.

15 [40] Zhao, C.; Yang, C. Electroosmotic flows of non-Newtonian power-law fluids in a  
16 cylindrical microchannel. *Electrophoresis* **2013**, *34*, 662–667.

17 [41] Afonso, A. M.; Alves, M. A.; Pinho, F. T. Analytical solution of mixed electro-  
18 osmotic/pressure driven flows of viscoelastic fluids in microchannels. *J. Non-Newton.*  
19 *Fluid Mech.* **2009**, *159*, 50–63.

1 [42] Afonso, A. M.; Alves, M. A.; Pinho, F. T. Analytical solution of two-fluid electro-osmotic  
2 flows of viscoelastic fluids. *J. Colloid Interface Sci.* **2013**, *395*, 277–286.

3 [43] Zimmerman, W. B.; Rees, J. M.; Craven, T. J. Rheometry of non-Newtonian electrokinetic  
4 flow in a microchannel T-junction. *Microfluid. Nanofluid.* **2006**, *2*, 481–492.

5 [44] Zhao, C.; Yang, C. Electro-osmotic mobility of non-Newtonian fluids. *Biomicrofluid.* **2011**,  
6 *5*, 014110.

7 [45] Zhao, C.; Yang, C. Exact solutions for electro-osmotic flow of viscoelastic fluids in  
8 rectangular micro-channels. *Appl. Math. Comput.* **2009**, *211*, 502–509.

9 [46] Park, H. M.; Lee, W. M. Helmholtz–Smoluchowski velocity for viscoelastic electroosmotic  
10 flows. *J. Colloid Interface Sci.* **2008**, *317*, 631–636.

11 [47] Zhao, C.; Zholkovskij, E.; Masliyah, J.; Yang, C. Analysis of electroosmotic flow of power  
12 law fluids in a slit microchannel. *J. Colloid Interf. Sci.* **2008**, *326*, 503–510.

13 [48] Olivares, M. L.; Vera-Candioti, L.; Berli, C. L. A. The EOF of polymer solutions.  
14 *Electrophoresis* **2009**, *30*, 921–929.

15 [49] Bello, M. S.; de Besi, P.; Rezzonico, R.; Righetti, P. G.; Casiraghi, E. Electroosmosis of  
16 polymer solutions in fused silica capillaries. *Electrophoresis* **1994**, *15*, 623–626.

17 [50] Chang, F. M.; Tsao, H. K. Drag reduction in electro-osmosis of polymer solutions. *Appl.*  
18 *Phys Lett.* **2007**, *90*, 194105.

19 [51] Mukherjee, S.; Das, S. S.; Dhar, J.; Chakraborty, S.; DasGupta, S. Electroosmosis of  
20 viscoelastic fluids: Role of wall depletion layer. *Langmuir* **2017**, *33*, 12046–12055

1 [52] Moschopoulos, P.; Dimakopoulos, Y.; Tsamopoulos, J. Electro-osmotic flow of electrolyte  
2 solutions of PEO in microfluidic channels. *J. Colloid Interface Sci.* **2020**, *563*, 381–393.

3 [53] Zhu, J.; Xuan, X. Dielectrophoretic focusing of particles in a microchannel constriction  
4 using DC-biased AC electric fields. *Electrophoresis* **2009**, *30*, 2668-2675.

5 [54] Lindner, A.; Bonn, D.; Meunier, J. Viscous fingering in a shear thinning fluid. *Phys. Fluids*  
6 **2000**, *12*, 256–261.

7 [55] Aytouna, M.; Paredes, J.; Shahidzadeh-Bonn, N.; Moulinet, S.; Wagner, C.; Amarouchene,  
8 Y.; Eggers, J.; Bonn, D. Drop formation in non- Newtonian fluids. *Phys. Rev. Lett.* **2013**,  
9 *110*, 034501.

10 [56] Henry, D. C. The cataphoresis of suspended particles. Part I – the equation of cataphoresis.  
11 *Proc. R. Soc. Lond. A* **1931**, *133*, 106–129.

12 [57] Xuan, X. Review of nonlinear electrokinetic flows in insulator-based dielectrophoresis:  
13 From induced charge to Joule heating effects. *Electrophoresis* **2022**, *43*, 167–189.

14 [58] Xuan, X. Joule heating in electrokinetic flow. *Electrophoresis* **2008**, *29*, 33-43.

15 [59] Bentor, J.; Dort, H.; Chitrapu, R.; Zhang, Y.; Xuan, X. Nonlinear electrophoresis of dielectric  
16 particles in Newtonian fluids. *Electrophoresis* **2023**, *44*, 938-946.

17 [60] Bentor, J.; Xuan, X.; Nonlinear electrophoresis of non-spherical particles in a rectangular  
18 microchannel. *Electrophoresis* **2024**, *45*, 712-719.

1 [61] Sze, A.; Erickson, D.; Ren, L.; Li, D. Zeta-potential measurement using the Smoluchowski  
2 equation and the slope of the current-time relationship in electroosmotic flow. *J. Colloid*  
3 *Interface Sci.* **2003**, *261*, 402–410.

4 [62] Malekanfard, A.; Ko, C. H.; Li, D.; Bulloch, L.; Baldwin, A.; Wang, Y. N.; Fu, L. M.; Xuan,  
5 X. Experimental study of particle electrophoresis in shear-thinning fluids. *Phys. Fluids*  
6 **2019**, *31*, 022002.

7 [63] Kirby, B. J.; Hasselbrink, E. F. Zeta potential of microfluidic substrates: 2. Data for  
8 polymers. *Electrophoresis* **2004**, *25*, 203.

9 [64] Uematsu, Y. Nonlinear electro-osmosis of dilute non-adsorbing polymer solutions with low  
10 ionic strength. *Soft Matt.* **2015**, *11*, 7402-7411.

11 [65] Matsuda, Y.; Sugiura, F.; Okumura, K.; Tasaka, S. Renaturation behavior of xanthan with  
12 high molar mass and wide molar mass distribution. *Polymer J.* **2016**, *48*, 653–658.

13 [66] Clavijo, J. V.; Moncayo-Riascos, I.; Husein, M.; Lopera, S. J.; Franco, C. A.; Cortés, F. B.  
14 Theoretical and experimental approach for understanding the interactions among SiO<sub>2</sub>  
15 nanoparticles, CaCO<sub>3</sub>, and xanthan gum components of water-based mud. *Energy Fuels*  
16 **2021**, *35*, 4803–4814.

17 [67] Lapizco-Encinas, B. H. The latest advances on nonlinear insulator-based electrokinetic  
18 microsystems under direct current and low-frequency alternating current fields: a review.  
19 *Anal. Bioanal. Chem.* **2022**, *414*, 885–905.

1 [68] Perez-Gonzalez, V. H. Particle trapping in electrically driven insulator-based microfluidics:

2 Dielectrophoresis and induced-charge electrokinetics. *Electrophoresis* **2021**, *42*, 2445–

3 2464.

4 [69] Lapizco-Encinas, B. H. Nonlinear electrokinetic methods of particles and cells. *Annu. Rev.*

5 *Anal. Chem.* **2024**, *17*, 243-264.

6

# 1 FOR TABLE OF CONTENTS ONLY

2

